# Non-diffusive transport in the tokamak edge pedestal

**W.M. Stacey**[1]**, R.J. Groebner**[2] **and T.E. Evans**[2]

[1] Georgia Institute of Technology, Atlanta, GA 30332, USA
[2] General Atomics, San Diego, CA 92186, USA

E-mail: weston.stacey@nre.gatech.edu

## Abstract

There are (at least) two classical mechanisms for non-diffusive transport in the edge plasma: (i) particle 'pinch' velocities due to forces such as $V \times B$ and $E_r$; and (ii) outward drifts due to ion-orbit loss and X-transport. A theoretical development for the treatment of these non-diffusive transport mechanisms within the context of fluid theory is assembled and applied to several DIII-D discharges in order to investigate the importance of these non-diffusive transport mechanisms in the edge pedestal. Several interesting insights emerge from this investigation.

(Some figures may appear in colour only in the online journal)

## 1. Introduction

It has long been recognized that an understanding of the physics of the tokamak edge plasma was important to achieving an understanding of tokamak performance, and tokamak edge pedestal physics has long been (e.g. [1]) and remains (e.g. [2]) an active area of tokamak physics research. The reason that it is important to understand the pedestal physics and to develop a predictive capability for the edge pedestal is that this physics seems to determine the performance of future tokamaks [3, 4], such as ITER.

A relationship between changes in the radial electric field $E_r$ and in the poloidal rotation velocity $V_\theta$ in the plasma edge, on one hand, and changes in the edge pressure, temperature and density gradients in the plasma edge, on the other hand, was one of the earliest experimental H-mode observations [5], suggesting that an understanding of the causes of the rotation velocities and the radial electric field may provide insight to an understanding of edge pedestal physics. Recently it has been demonstrated that changes in these various experimentally observed quantities are correlated by momentum balance requirements [6–8].

Although there is a growing consensus that the limiting values of pedestal pressure and pressure gradients are determined by magnetohydrodynamic (MHD) peeling-ballooning mode instabilities [9] (edge localized modes or ELMs), the causes of the pedestal structure (pressure, density and temperature profiles) in the absence of ELMs or between ELMs remain an open question. One widely held school of thought (e.g. [10–12]) postulates that the stabilization of electromagnetic micro-instabilities and the corresponding reduction in fluctuation-driven transport coefficients produce the observed steepening in temperature and density gradients in order for diffusive heat and particle fluxes to remove the input heat and particles. Another school of thought (e.g. [13–28]) postulates that the physics of the edge plasma is determined, at least in part, by the free-streaming ion-orbit loss and drift loss of thermal ions trapped poloidally in the region near the X-point that drift across the separatrix and into the divertor. Ionization of recycling neutral atoms [29, 30] and small-scale kinetic ballooning mode MHD instabilities [31] also have been suggested as causes of the observed structure in the density and temperature profiles in the edge pedestal of tokamak plasmas.

There are a large number of people worldwide working to understand edge pedestal physics and to test these various postulated causes of the edge pedestal structure against experimental data. Much of this work consists of comparing measured temperature and density profiles in the edge pedestal with the predictions of 1D or 2D fluid transport codes which incorporate various theoretical models for the transport coefficients, or using such codes to calculate particle and heat fluxes that can be used to interpret experimental values of the transport coefficients from the measured density and temperature profiles. For example, the National H-Mode Edge Pedestal (HEP) Group [32] has compared DIII-D edge data with 1D codes such as ONETWO [33], ASTRA [34] and GTEDGE [35], and with 2D codes such as UEDGE [36] and SOLPS [37]; and extensive tests of theoretical models against experimental data have been reported in the literature (e.g. [32, 38]).

However, such analyses usually do not take into account the non-diffusive transport effects of forces due the electric

1

fields and $V \times B$ forces (which produce a particle pinch), nor do they usually take into account non-diffusive ion-orbit losses and drift X-transport. Thus, we have been motivated to assemble a fluid transport theory for the edge plasma that systematically incorporates these non-diffusive transport processes. Another purpose of this paper is to illustrate the importance of taking into account these non-diffusive transport mechanisms by application of this extended fluid transport theory to the interpretation of the edge plasma physics in several different types of DIII-D [39] discharges.

## 2. A moments equation formulation of plasma fluid theory in a tokamak

In this section, plasma fluid theory is formulated systematically from the first four velocity moments of the Boltzman transport equation [40], with appropriately determined constitutive relations (transport coefficients). In order to simplify the formalism, one-dimensional radial transport in a slab approximation is used.

The first velocity moment is the particle density, and the first velocity moment equation is the continuity, or particle balance, equation for the main ion species '$j$':

$$\frac{\partial (n_j V_{rj})}{\partial r} = -\frac{\partial n_j}{\partial t} + n_e n_o \langle \sigma \upsilon \rangle_{\text{ion}} + S_{\text{nb}}, \qquad (1)$$

which includes also the second velocity moment, $V_{rj}$, the average radial ion fluid velocity, in the form of the radial particle flux $\Gamma_j = n_j V_{rj}$. The second term on the right is the ionization of recycling neutrals and the last term is the neutral beam source. Similar equations obtain for other ion species '$k$' present in the plasma, and the electron density is constrained by quasi-neutrality.

The toroidal and radial components of the second velocity moment, or momentum balance, equation may be written for any ion species '$j$':

$$n_j m_j [(\nu_{jk} + \nu_{dj}) V_{\phi j} - \nu_{jk} V_{\phi k}]$$
$$= n_j e_j E_\phi^A + n_j e_j B_\theta V_{rj} + M_{\phi j} \qquad (2)$$

and

$$V_{\phi j} = \frac{1}{B_\theta} \left[ E_r + V_{\theta j} B_\phi - \frac{1}{n_j e_j} \frac{\partial p_j}{\partial r} \right], \qquad (3)$$

where '$k$' in general refers to a sum over other ion species. In this paper '$j$' will refer to the main ion (deuterium) and '$k$' to the impurity ion (carbon) in a two-species model. These equations contain the third velocity moment of the distribution function, the pressure (or equivalently the temperature).

The quantity $\nu_{dj}$ is a toroidal angular momentum transfer frequency which represents the combined effect of viscosity, inertia, atomic physics and other 'anomalous' processes. Justification for representing the toroidal momentum transfer processes in this form is discussed in appendix A and in [41]. $M_{\phi j}$ is the toroidal momentum input, $e_j$ refers to the charge of species '$j$' and the other symbols have their usual meaning.

Subject to the assumption that there is a single impurity species '$k$' with the same logarithmic density derivative and the same local temperature as the main ions '$j$', equations (2)

and (3) can be combined to arrive at a constraint on the main ion pressure gradient

$$-\frac{1}{p_j} \frac{\partial p_j}{\partial r} = \frac{V_{rj} - V_{rj}^{\text{pinch}}}{D_j}, \qquad (4)$$

where the 'diffusion coefficient' is

$$D_j \equiv \frac{m_j T_j \nu_{jk}}{(e_j B_\theta)^2} \left( 1 + \frac{\nu_{dj}}{\nu_{jk}} - \frac{e_j}{e_k} \right) \qquad (5)$$

and the 'pinch velocity'

$$V_{rj}^{\text{pinch}} = [-M_{\phi j} - n_j e_j E_\phi^A + n_j m_j (\nu_{jk} + \nu_{dj})$$
$$\times (f_p^{-1} V_{\theta j} + E_r / B_\theta) - n_j m_j \nu_{jk} V_{\phi k}][n_j e_j B_\theta]^{-1} \qquad (6)$$

is a collection of normalized forces associated with the electric field, $V \times B$ forces and beam momentum input. The fundamental transport coefficients that determine the main ion diffusion coefficient are the momentum exchange frequencies with impurities ($\nu_{jk}$) and with neutrals ($\nu_{cx}$), and the momentum exchange frequencies across flux surfaces due to viscosity and inertia, and any anomalous momentum exchange processes (included in $\nu_{dj}$).

Experimental values of the toroidal angular momentum transfer frequencies $\nu_{dj}$ and $\nu_{dk}$ can be inferred from equations (2) and (3) by using the measured carbon toroidal rotation velocity and making a perturbation analysis to estimate the main ion toroidal rotation velocity [42, 43].

$$\nu_{dj} =$$
$$\frac{(n_j e_j E_\phi^A + e_j B_\theta \Gamma_j + M_{\phi j}) + (n_k e_k E_\phi^A + e_k B_\theta \Gamma_k + M_{\phi k})}{(n_j m_j + n_k m_k) V_{\phi k}^{\text{exp}}} \qquad (7)$$

and for the carbon impurity ion

$$\nu_{dk} = \frac{(n_k e_k E_\phi^A + e_k B_\theta \Gamma_k + M_{\phi k}) + n_j m_j \nu_{jk} (V_{\phi j} - V_{\phi k})_0}{n_k m_k V_{\phi k}^{\text{exp}}}, \qquad (8)$$

where

$$(V_{\phi j} - V_{\phi k})_0 = \frac{(n_j e_j E_\phi^A + e_j B_\theta \Gamma_j + M_{\phi j}) - n_j m_j \nu_{dj} V_{\phi k}^{\text{exp}}}{n_j m_j (\nu_{jk} + \nu_{dj})} \qquad (9)$$

is the first order perturbation estimate of the difference in deuterium and carbon toroidal rotation velocities.

The momentum balance requirement of equation (4) can be rearranged into a form that clearly exhibits the diffusive and the non-diffusive components of the radial particle flux

$$\Gamma_j \equiv n_j V_{rj} = -\frac{n_j D_j}{p_j} \frac{\partial p_j}{\partial r} + n_j V_{rj}^{\text{pinch}}$$
$$= -D_j \frac{\partial n_j}{\partial r} - D_j \frac{n_j}{T_j} \frac{\partial T_j}{\partial r} + n_j V_{rj}^{\text{pinch}}. \qquad (10)$$

The more general case when the assumption made above about the impurity distribution is not made is treated in appendix B.

The third velocity moment, or energy balance, equations for the main ion and electron species

$$\frac{\partial Q_j}{\partial r} \equiv \frac{\partial}{\partial r} \left( q_j + \frac{3}{2} \Gamma_j T_j \right) = -\frac{\partial}{\partial t} \left( \frac{3}{2} n_j T_j \right) + q_{\text{nb}j} - q_{je}$$
$$-n_e n_o^c \langle \sigma \upsilon \rangle_{\text{cx}} \frac{3}{2} (T_j - T_o^c) \qquad (11)$$

and

$$\frac{\partial Q_e}{\partial r} \equiv \frac{\partial}{\partial r} \left( q_e + \frac{3}{2} \Gamma_e T_e \right)$$
$$= -\frac{\partial}{\partial t} \left( \frac{3}{2} n_e T_e \right) + q_{nbe} + q_{je} - n_e n_k L_k(T_e) \quad (12)$$

determine the main ion and electron total energy fluxes $Q_{j,e}$. The $q_{nb}$ terms represent neutral beam (or other) heating, $q_{je}$ is the ion-to-electron collisional energy transfer, and the last terms in equations (11) and (12) represent charge-exchange cooling of the ions and radiation cooling of the electrons, respectively. These equations contain the fourth velocity moment of the distribution function, the conductive heat fluxes $q_{j,e}$.

In principle, the fourth moment equations could be solved for the conductive heat fluxes, $q_{j,e}$, but these equations are rather formidable [40], involving complex tensor differential relations among the lower velocity moments and the next higher, fifth order velocity moment of the distribution function. In practice, these fourth order velocity moment equations are replaced by the surrogate equations

$$q_{j,e} = -n_{j,e} \chi_{j,e} \frac{\partial T_{j,e}}{\partial r}, \quad (13)$$

which can be used to determine the temperature profiles, thus closing the set of four moments equations.

It should be recognized that replacing the actual fourth velocity moment equation by equation (13) is equivalent (in a sense) to neglecting the last two (temperature gradient and pinch) terms in the second velocity moment equation (10), which would close the first two moments equations and lead to the familiar particle diffusion theory upon such truncation of equation (10) and substitution into the continuity equation. Thus, we might expect that using equation (13) instead of the fourth velocity moment equation ignores some 'energy pinch' terms as well as some differential relations involving a fifth velocity moment of the distribution function as well as other velocity moments. Investigation of the retention of such terms would be of great interest, however, development of such an extended formalism is well beyond the scope of the present investigation or the present state of the art.

In an interpretive analysis, the experimental values of the thermal diffusivities can be inferred [38] from the respective density and temperature profiles

$$\chi_{j,e}^{exp} = -\frac{q_{j,e}^{exp}}{n_{j,e}^{exp}(\partial T_{j,e}^{exp}/\partial r)} = -\frac{(Q_{j,e}^{exp} - 1.5\Gamma_{j,e}^{exp}T_{j,e}^{exp})}{n_{j,e}^{exp}(\partial T_{j,e}^{exp}/\partial r)} \quad (14)$$

when $Q_{j,e}^{exp}$ is obtained by solving equation (11) or (12) for the total heat flux, $\Gamma_j^{exp}$ is obtained by solving equation (1) for the total radial particle flux and $\Gamma_e^{exp}$ is constructed therefrom taking into account impurities.

## 3. Non-diffusive particle transport (pinch) effects in DIII-D experiments

The above equations can be used to investigate the importance of the $V \times B$ and $E_r$ 'pinch' forces that appear in the momentum balance requirement of equation (10) in various types of discharges.
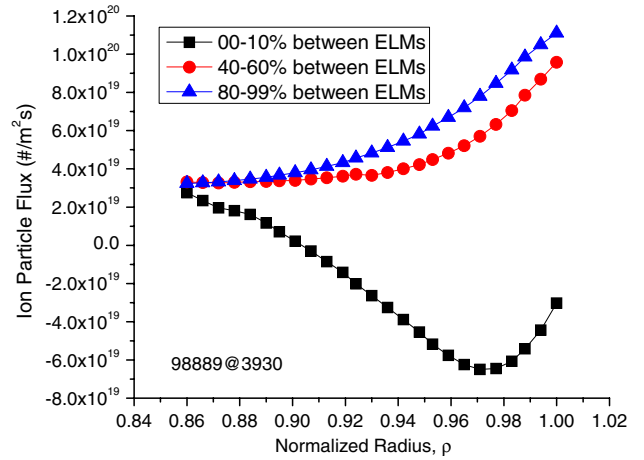


**Figure 1.** Ion particle flux evaluated from equation (1) for DIII-D shot #98889.
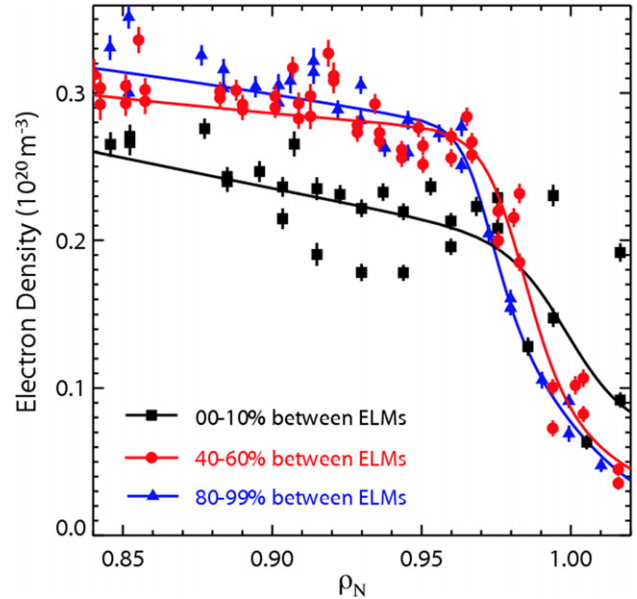


**Figure 2.** Experimental electron density in DIII-D shot #98889.

*3.1. Evolution of H-mode edge pedestal between ELMs*

Experimental data were averaged over the same sub-intervals between ELMs for successive ELMs to develop data that characterize the evolution of density, temperature, rotation velocities, radial electric field, etc over the interval between ELMs in DIII-D shot #98889. These data [7] provide an experimental confirmation of an inward particle pinch.

The ion particle fluxes at several times after an ELM, obtained by solving equation (1) using experimental values to evaluate the parameters, are shown in figure 1. Immediately following the ELM (0–10%), the net radial particle flux is inward over the edge plasma, but recovers to an outward flux by midway (40–60%) between ELMs. The deuterium ion density radial distribution was calculated to be very close to the measured electron density distribution shown in figure 2, and the evolution of the radial temperature distributions for ions and electrons were similar to that of the electron density shown in figure 2.
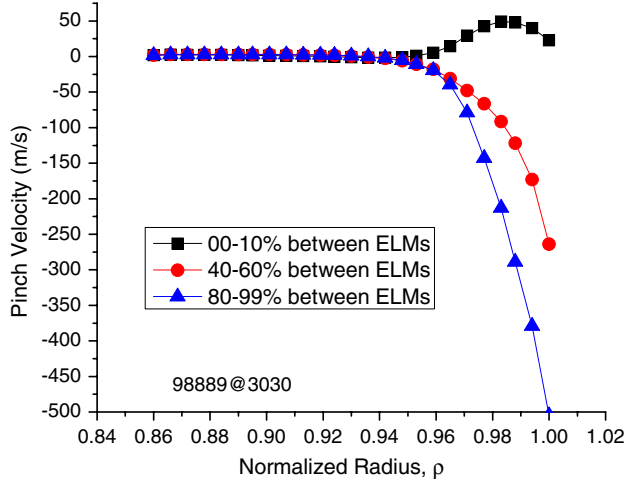
**Figure 3.** Pinch velocity of equation (6) evaluated with experimental parameters.
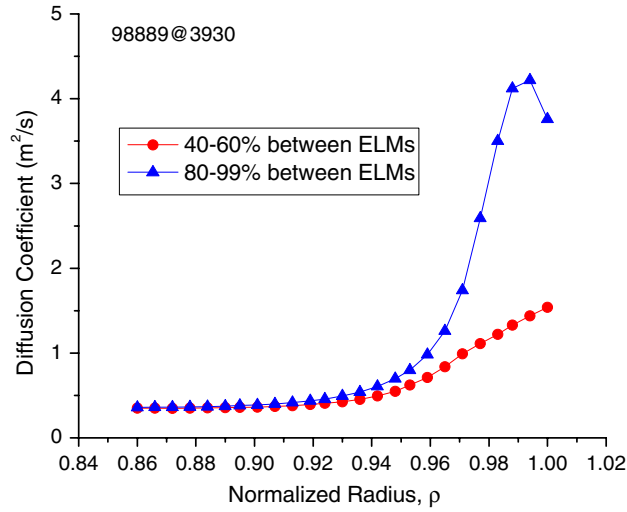


**Figure 4.** Diffusion coefficient of equation (5) evaluated with experimental data.

With respect to the momentum balance requirement on the radial ion particle flux given by equation (10), it is clear that the outward diffusive fluxes (both the density gradient and temperature gradient terms) cannot account for the inferred inward particle flux immediately following the ELM (0–10%) but that an inward pinch term is required. The pinch velocity inferred by using experimental data to evaluate equation (6) is shown in figure 3. Unfortunately, the averaging period for the CER data used to evaluate rotation and radial electric field terms in equation (6) is longer than the (0–10%) interval between ELMs, which means that this interval contains some pre-ELM and ELM CER data, which is probably the cause of the outward pinch velocity predicted by equation (6) in the (0–10%) interval. More likely the pinch velocity just after the ELM is small but inward. (We intend to revisit this issue on a shot with better resolved CER data.)

The diffusion coefficient of equation (5) evaluated with experimental parameters, shown in figure 4, increases with time between ELMs. Since the density gradient of figure 2 is also increasing with time, we conclude that the outward
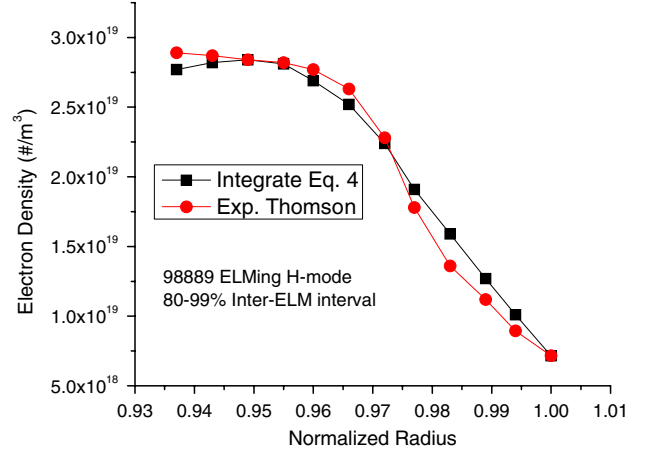


**Figure 5.** Comparison of measured and calculated ion density profile in edge pedestal.

diffusive component of the radial particle flux increases significantly from just after an ELM to just before the next ELM, while figure 3 indicates that the inward (pinch velocity) non-diffusive radial particle flux also increases significantly between ELMs. The relatively smaller net particle flux of figure 1 is the difference between larger outward diffusive and inward non-diffusive fluxes.

### 3.2. Consistency check

If the viscous component of the angular momentum transfer frequencies $\nu_{dj,k}$ and the thermal diffusivities $\chi_{j,e}$ were known, from kinetic theory or fluctuation theory or experiment, it should be possible to solve equation (4) for the ion pressure distribution and equation (13) for the ion temperature distribution, then construct the ion distribution from $n_j = p_j/T_j$. As a surrogate for knowing the transport coefficients, we have inferred $\nu_{dj,k}$ from experiment using equations (7)–(9) and used the measured ion temperature. Then equation (4) was integrated to obtain $p_j(r)$, which was then divided by the experimental $T_j$ and corrected for impurities to obtain the electron density distribution shown by the square symbols in figure 5. The result is very close to the measured (Thomson scattering) electron density in the outer part of the edge pedestal where the slab geometry approximation used in the integration of equation (4) is valid.

### 3.3. Relative importance of recycling neutrals and 'pinch' forces in determining edge pedestal density profile

The effect of the $V \times B$, $E_r$ and other 'pinch' forces on the determination of the pressure profile from equation (4) enters through the term $V_{rj}^{\text{pinch}}$, which was evaluated mostly from experimental data. The effect of recycling neutrals on the determination of the pressure profile from equation (4) enters through the term $V_{rj}$, which is evaluated by solving the continuity equation (1) using the experimental density profile. (The recycling neutrals also affect the diffusion coefficient in the denominator of equation (4) via the charge-exchange contribution to $\nu_{dj}$, but this charge-exchange contribution generally has been found to be less than 10% just inside the separatrix and even less further in.) Thus, comparing these
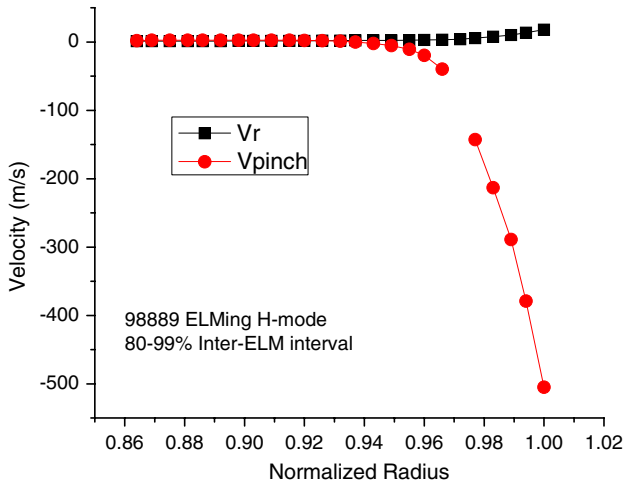
**Figure 6.** Comparison of the importance of recycling neutrals ($V_r$) and $V \times B$ and $E_{rad}$ ($V_{pinch}$) in determining the pressure gradient in the edge pedestal.
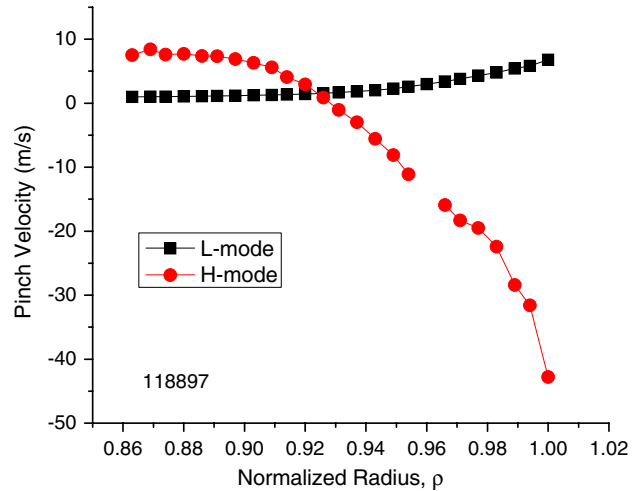


**Figure 8.** Comparison of pinch velocities in L-mode and H-mode phases of DIII-D shot #118897.
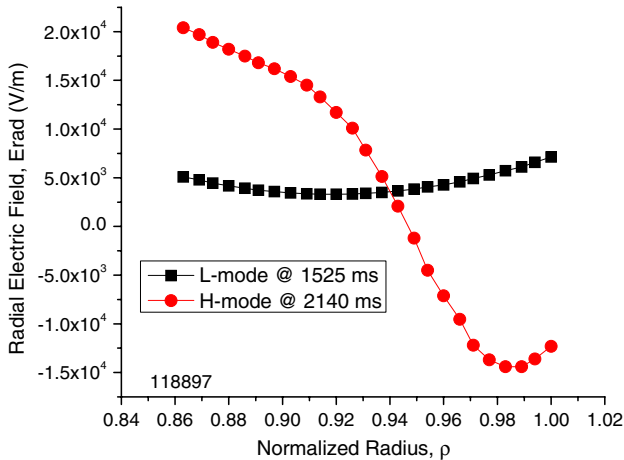


**Figure 7.** Radial electric in L-mode and H-mode phases of DIII-D shot #118897.



**Figure 9.** Main ion diffusion coefficients in L- and H-mode phases of DIII-D. Shot #118897.

two terms in figure 6 provides an appreciation of the relative importance of (i) recycling neutrals and (ii) $V \times B$, $E_r$ and other 'pinch' forces on the determination of the pressure profile. Similar results have been found for other DIII-D discharges, indicating that the pinch velocity effects generally dominate the neutral recycling effects in the determination of the edge pressure and density profiles.

### 3.4. Differences in L-mode and H-mode edge plasmas

It has long been noted that, in addition to differences in the temperature and density distributions, there was a difference in the radial electric field distributions between L-mode and H-mode plasmas [5]. The radial electric fields in the L-mode and early (pre-ELM) H-mode phases of DIII-D shot #118897 are markedly different, as shown in figure 7. This difference in radial electric fields, and lesser differences in poloidal rotation velocities, lead to dramatically different non-diffusive radial pinch velocities, as shown in figure 8. In the L-mode phase the principal non-diffusive radial particle flux (pinch velocity) components due to the radial electric field and due to the
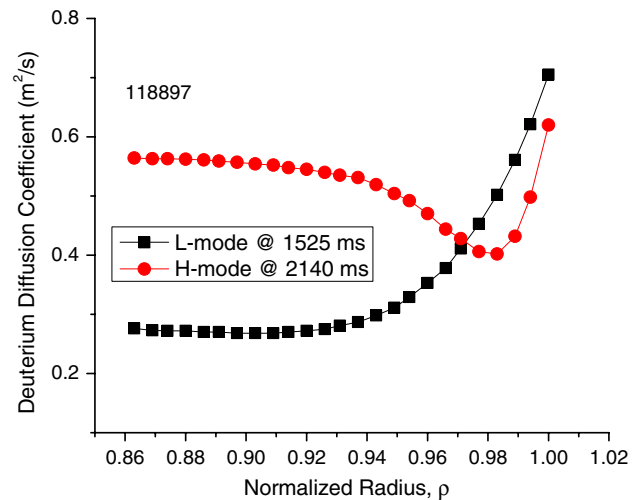
poloidal rotation velocity are of opposite signs and tend to cancel each other, resulting in a small outward non-diffusive (pinch) radial particle flux. On the other hand, for the H-mode phase the poloidal velocity and radial electric field components are both inward and reinforce one another to produce a strong inward non-diffusive (pinch) radial particle flux component. (The deuterium poloidal velocity needed for this evaluation was calculated from poloidal momentum balance, using the measured carbon rotation velocity.)

The diffusion coefficients of equation (5), evaluated from experimental data as described above for shot #98889, are plotted for the L-mode and H-mode phases of shot #118897 in figure 9. These diffusion coefficients are comparable in the steep-gradient region, indicating that the diffusive component of the radial particle flux through the steep-gradient region is actually larger for the H-mode phase (because of the steeper density gradient) than for the L-mode phase. Thus, relative to the L-mode phase, the steeper density (and pressure) gradient in the H-mode phase would appear to be required by momentum balance in order to offset the larger inward non-diffusive particle flux and enable the net outward particle flux required by particle balance to be achieved.
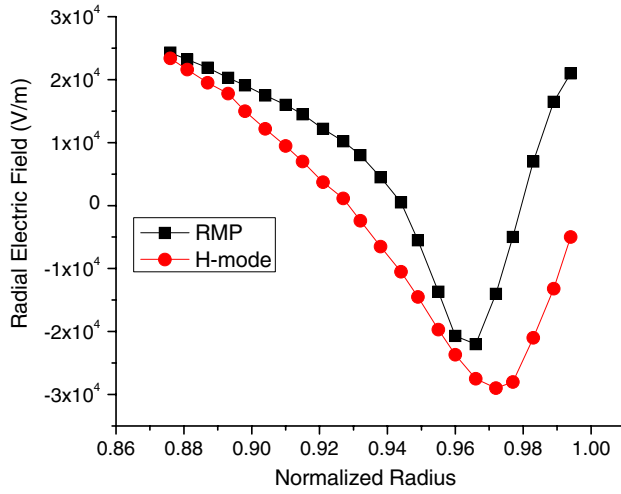
**Figure 10.** Radial electric fields in matching RMP and H-mode DIII-D shots.

*3.5. The effects of resonant magnetic perturbations on the edge plasma*

Resonant magnetic perturbations (RMPs) appear to suppress ELMs by reducing edge particle density below the pressure limit for ballooning-peeling modes. We have investigated the role of non-diffusive particle transport in this RMP ELM-suppression by evaluating differences in the pinch velocity of equation (6) and in the diffusion coefficient of equation (5) from the experimental data [8] for a matched pair of H-mode and RMP shots in DIII-D. Except for the RMP, these shots had identical operating parameters. The edge density in the RMP shot was about half that in the H-mode shot, the ion temperature in the RMP shot was about twice that in the H-mode shot, and the electron temperatures were very similar.

Another interesting difference between these two discharges was in the radial electric field profiles shown in figure 10. The H-mode radial electric field is negative in the steep-gradient region with the characteristic deep well just inside the separatrix. The radial electric field in the RMP discharge has not quite as deep a negative dip and becomes positive in the outermost pedestal inside the separatrix.

These different radial electric fields (and poloidal rotation velocities) produce rather different non-diffusive particle fluxes, as indicated by the pinch velocities shown in figure 11. The strongly inward non-diffusive pinch velocity in the steep-gradient region of the H-mode shot is reduced in the RMP shot.

The diffusion coefficients of equation (5) are comparable for the RMP and H-mode shots, except at the separatrix, as shown in figure 12. Since the density gradients are steeper in the edge for the H-mode shot, the outward diffusive particle fluxes over most of the edge are larger for the H-mode shot than for the RMP shot.

Thus, it would seem that a significant contributing mechanism for edge density reduction with RMP is the reduction of the large inward non-diffusive (pinch) particle flux in the edge relative to H-mode.

## 4. Generalized diffusion theory

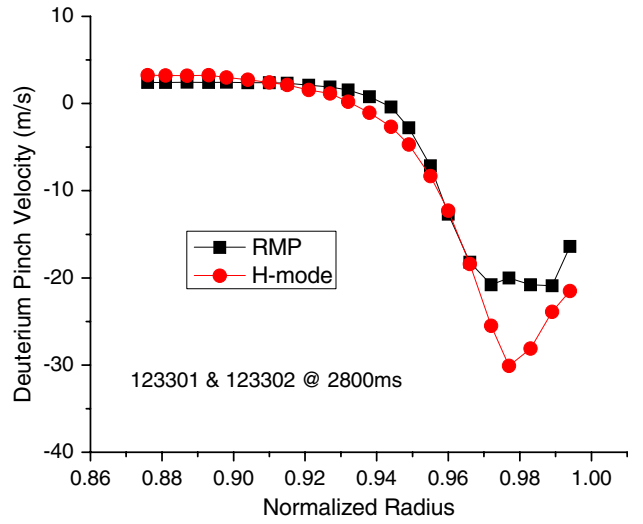If the momentum balance constraint of equation (10) is substituted into the continuity equation (1), a generalized



**Figure 11.** Non-diffusive radial pinch velocities of equation (6) for the RMP and H-mode shots.
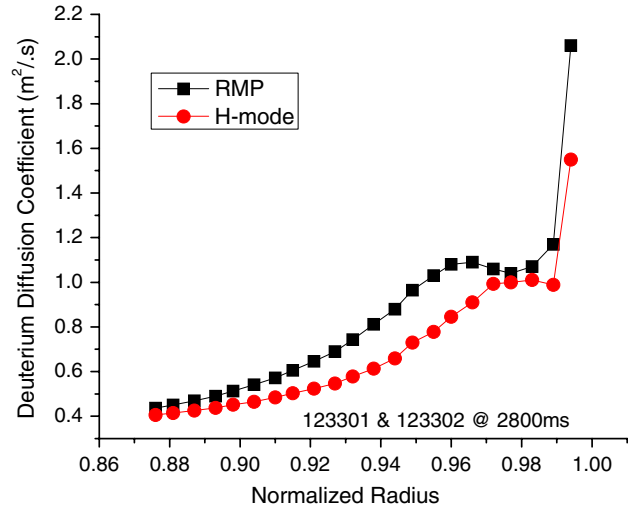


**Figure 12.** Diffusion coefficients of equation (5) for the RMP and H-mode shots.

diffusion equation is obtained.

$$-\frac{\partial}{\partial r}\left(D_j\frac{\partial n_j}{\partial r}\right) - \frac{\partial}{\partial r}\left(D_j\frac{n_j}{T_j}\frac{\partial T_j}{\partial r}\right) + \frac{\partial(n_j V_{rj}^{\text{pinch}})}{\partial r}$$
$$= -\frac{\partial n_j}{\partial t} + S_j \equiv -\frac{\partial n_j}{\partial t} + n_e n_o\langle\sigma\upsilon\rangle_{\text{ion}} + S_{\text{nb}} \quad (15)$$

under the same assumption used above that the logarithmic derivatives of the impurity and main ion density profiles are the same. (The more general case is treated in [41] and appendix C.) Solving equations (1) and (15) for the density and radial velocity profiles should result in the same profiles that would be obtained by solving equation (1) and equation (4) or (10) (the relative accuracy of numerical approximations to equations (4) and (15) is discussed in [44]).

It is common practice in many codes used for edge plasma analysis to use equations (1) and (15), but with the second 'temperature diffusion' term and the third 'pinch velocity' term omitted in the latter, and with a diffusion coefficient that is adjusted to match experimental density profiles. This

is equivalent to representing the particle flux by only the first diffusive term on the left-hand side of equation (10) and adjusting the diffusion coefficient to compensate for the omission of the last two (temperature gradient and pinch) terms on the left-hand side. Such a process can lead to extremely small and physically meaningless adjusted diffusion coefficients (e.g. [32]) in the presence of the large inward pinch velocities found in the edge plasma in the previous section 3. These small values of the adjusted diffusion coefficients have been interpreted as an 'edge particle transport barrier', but it is clear that they are just an artefact of the non-physical fitting procedure. The better particle confinement in H-mode would seem to be associated with a larger inward particle pinch, not with a reduced diffusion coefficient, in the discharges investigated.

## 5. Non-diffusive ion transport due to ion-orbit loss and X-transport

There are (at least) two other classical mechanisms for non-diffusive ion transport in the edge plasma. The most familiar is the case of ions on passing or banana-trapped orbits that leave the plasma by drifting outward across the last closed flux surface (e.g. [14, 19, 20, 27, 45, 46]), where they are assumed either to be charge-exchanged or to intersect a material surface and not re-enter the plasma. Both thermal plasma ions and energetic neutral beam ions (and fusion alpha particles) can be lost in this manner.

A second ion transport loss mechanism, more recently elaborated by Chang and colleagues [21–26] and one of us [28], is an outward drift transport through the region near the X-point in diverted plasmas. Ions on spiraling orbits that pass near the X-point where the poloidal magnetic field is very small have a very small poloidal displacement in time and are essentially trapped in the poloidal vicinity of the X-point, where they are subject to vertical curvature and grad-$B$ drifts which take them outward until they either drift out across the separatrix near the X-point or $E_r \times B_\phi$ drift poloidally out of the low poloidal field region. The poloidal motion of the electrons is sufficient that they are not affected by this trapping mechanism, so there is effectively a radially outward ion current which builds up an inward-directed radial electric field. This radial electric field interacts with the toroidal magnetic field to produce a $E_r \times B_\phi$ poloidal drift that de-traps the ions by allowing them to drift poloidally onto spiraling field lines that are not trapped in the vicinity of the X-point. Thus, this X-transport rate is determined by the relative values of the vertical curvature and grad-$B$ drift loss rate and of the de-trapping $E_r \times B_\phi$ poloidal drift rate. (Note that X-transport will be treated in the fluid theory as a convection from one radius to a larger one; only if the X-transport carries the ion across the separatrix is it lost.)

Both of these mechanisms are essentially kinetic, non-diffusive transport mechanisms. Computationally tractable models for their evaluation and incorporation into the above fluid transport calculation are set out in the following.

### 5.1. Ion-orbit loss model and application to DIII-D

We make use of the conservation of canonical toroidal angular momentum

$$RmV_\| f_\varphi + e\psi = \text{const} = R_0 mV_{\|0} f_{\varphi 0} + e\psi_0 \quad (16)$$

to write the orbit constraint for an ion introduced at a location '0' on flux surface $\psi_0$ with parallel velocity $V_{\|0}$, where $f_\varphi = |B_\varphi/B|$, $R$ is the major radius and $\psi$ is the flux surface value. The conservation of energy and of poloidal angular momentum

$$\frac{1}{2}m(V_\|^2 + V_\perp^2) + e\phi = \text{const} = \frac{1}{2}m(V_{\|0}^2 + V_{\perp 0}^2) + e\phi_0$$

$$\equiv \frac{1}{2}mV_0^2 + e\phi_0$$

$$\frac{mV_\perp^2}{2B} = \text{const} = \frac{mV_{\perp 0}^2}{2B_0} \quad (17)$$

further require

$$V_\| = \pm V_0 \left[ 1 - \left| \frac{B}{B_0} \right| (1 - \zeta_0^2) + \frac{2e}{mV_0^2}(\phi - \phi_0) \right]^{1/2}, \quad (18)$$

where $\phi$ is the electrostatic potential. The quantity $\zeta_0 = V_{\|0}/V_0$ is the cosine of the initial guiding centre velocity relative to the toroidal magnetic field direction.

Using equation (18) in equation (16) and squaring leads to a quadratic equation in the initial ion velocity $V_0 = \sqrt{V_{\|0}^2 + V_{\perp 0}^2}$:

$$V_0^2 \left[ \left( \left| \frac{B}{B_0} \right| \frac{f_{\varphi 0}}{f_\varphi} \zeta_0 \right)^2 - 1 + (1 - \zeta_0^2) \left| \frac{B}{B_0} \right| \right]$$

$$+ V_0 \left[ \frac{2e(\psi_0 - \psi)}{Rmf_\varphi} \left( \left| \frac{B}{B_0} \right| \frac{f_{\varphi 0}}{f_\varphi} \zeta_0 \right) \right]$$

$$+ \left[ \left( \frac{e(\psi_0 - \psi)}{Rmf_\varphi} \right)^2 - \frac{2e(\phi_0 - \phi)}{m} \right] = 0. \quad (19)$$

Note that equation (19) is quite general with respect to flux surface geometry representation of $R$, $B$ and the flux surfaces $\psi$. By specifying an initial '0' location for an ion with initial direction cosine $\zeta_0$, and specifying a final location on flux surface $\psi$, equation (19) can be solved for the minimum initial ion speed $V_0$ that is required in order for the ion orbit to reach the final location. Thus, equation (19) can be solved for the minimum ion energy necessary for an ion located on an internal flux surface to cross the last closed flux surface at a given location or to strike the chamber wall at a given location, etc. All of the particles with energy greater than this $V_{0\,\text{min}}(\zeta_0)$ are lost across the last closed flux surface (and assumed in this work not to return) or strike the chamber wall. The quantity $V_{0\,\text{min}}(\zeta_0)$ is very large for particles with parallel velocity opposite to the direction of the toroidal magnetic field ($\zeta_0 < 0$), which execute banana orbits inside the flux surface, but becomes smaller with increasing $\zeta_0 > 0$ (i.e. as the particle velocity becomes more nearly aligned with the toroidal magnetic field direction).

Since $V_{0\,\text{min}}(\zeta_0)$ decreases with radius, cumulative (with increasing radius) particle, momentum and energy loss fractions can be defined

$$F_{\text{orb}} \equiv \frac{N_{\text{loss}}}{N_{\text{tot}}} = \frac{\int_{-1}^{1} \left[ \int_{V_{0\,\text{min}(\zeta_0)}}^{\infty} V_0^2 f(V_0)\, dV_0 \right] d\zeta_0}{2 \int_0^\infty V_0^2 f(V_0)\, dV_0}$$

$$= \frac{\int_{-1}^{1} \Gamma(\frac{3}{2}, \varepsilon_{\text{min}(\zeta_0)})\, d\zeta_0}{2\Gamma(\frac{3}{2})}, \quad (20)$$
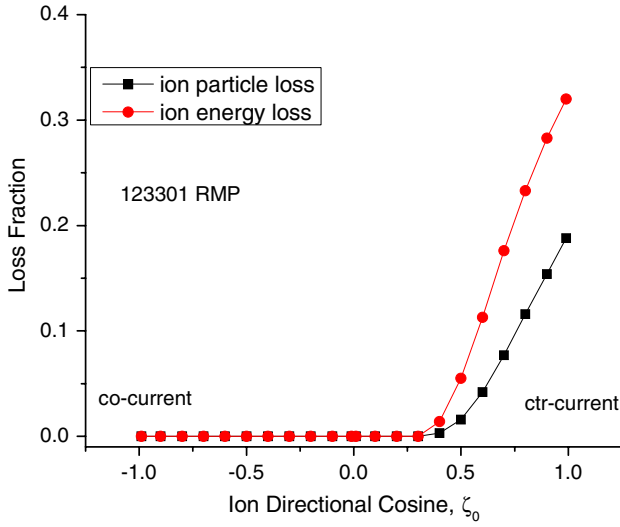
**Figure 13.** Angular particle and energy ion-orbit loss fractions for RMP discharge.



**Figure 14.** Ion particle and energy cumulative loss fractions for ion-orbit loss in DIII-D RMP and otherwise similar H-mode discharges.

$$M_{\text{orb}} \equiv \frac{M_{\text{loss}}}{M_{\text{tot}}} = \frac{\int_{-1}^{1} \left[ \int_{V_{0\min(\zeta_0)}}^{\infty} (m V_0) V_0^2 f(V_0) \, dV_0 \right] d\zeta_0}{2 \int_{0}^{\infty} (m V_0) V_0^2 f(V_0) \, dV_0}$$

$$= \frac{\int_{-1}^{1} \Gamma(2, \varepsilon_{\min(\zeta_0)}) \, d\zeta_0}{2\Gamma(2)} \tag{21}$$

and

$$E_{\text{orb}} \equiv \frac{E_{\text{loss}}}{E_{\text{total}}} = \frac{\int_{-1}^{1} \left[ \int_{V_{0\min(\zeta_0)}}^{\infty} \left( \frac{1}{2} m V_0^2 \right) V_0^2 f(V_0) \, dV_0 \right] d\zeta_0}{\int_{-1}^{1} \left[ \int_{0}^{\infty} \left( \frac{1}{2} m V_0^2 \right) V_0^2 f(V_0) \, dV_0 \right] d\zeta_0}$$

$$= \frac{\int_{-1}^{1} \Gamma\left(5/2, \varepsilon_{\min(\zeta_0)}\right) d\zeta_0}{2\Gamma(\frac{5}{2})}, \tag{22}$$

where $\varepsilon_{\min}(\zeta_0) = m V_{0\min}^2(\zeta_0)/2kT$ is the reduced energy corresponding to the minimum velocity for which ion-orbit loss is possible, and an initially Maxwellian ion distribution has been assumed. The quantities $\Gamma(n)$ and $\Gamma(n, x)$ are the gamma function and incomplete gamma function.

The particle and energy angular loss fractions, $\Gamma(3/2, \varepsilon_{\min(\zeta_0)})/2\Gamma(3/2)$ and $\Gamma(5/2, \varepsilon_{\min(\zeta_0)})/2\Gamma(5/2)$, are plotted as a function of the direction cosine of the particle velocity with respect to the toroidal magnetic field in figure 13. (The momentum loss fraction, $\Gamma(2, \varepsilon_{\min(\zeta_0)})/2\Gamma(2)$, is intermediate.) Clearly, it is the particles with velocities along the toroidal magnetic field direction (which execute banana orbits outside the flux surface) that are preferentially lost. The loss fractions for the H-mode discharge were similar but somewhat different quantitatively.

These cumulative particle and energy loss fractions, obtained by integrating the angular loss fractions of figure 13 over angle, are plotted in figure 14 for the matched pair of RMP (#123301) and H-mode (#123302) shots discussed above (the momentum loss fractions are intermediate between the particle and energy loss fractions). The difference in the radial electric fields shown in figure 10 and the larger ion temperature (by a factor of 2) in the RMP shot accounts for the much larger cumulative ion-orbit loss for the RMP shot than for the otherwise similar H-mode shot. These loss fractions do not change the total particle and ion heat fluxes calculated
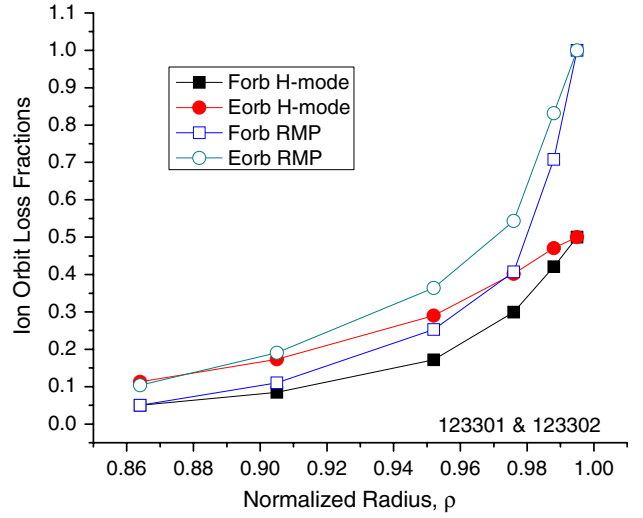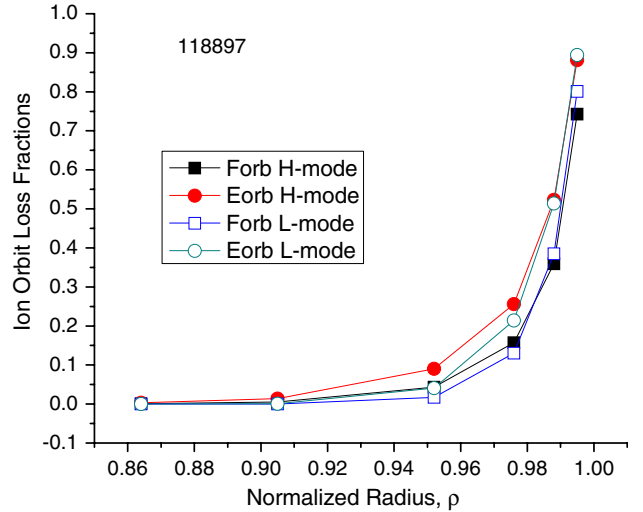


**Figure 15.** Ion-orbit particle and energy cumulative loss fractions for the L- and H-mode phases of DIII-D shot 118897.

by the fluid model, but rather represent the fraction of these total particle and energy fluxes at each radial position that are in the form of free-streaming ions that escape across the separatrix without being involved in other plasma conductive and convective transport processes.

The ion-orbit loss calculation was repeated for the L-mode and early (ELM-free) H-mode phases of DIII-D shot 118897, using the corresponding experimental density and temperature data and the measured radial electric fields of figure 7 in solving equation (19). The resulting particle and energy ion-orbit loss fractions shown in figure 15 are rather similar for the L- and H-mode phases, indicating a smaller effect of the radial electric field profile than was found in the RMP and H-mode shot comparison above.

### 5.2. X-transport model and application to DIII-D

In a region about the X-point the poloidal field is very small, $B_\theta \ll \varepsilon B_\phi$, and the field lines are almost purely toroidal and do
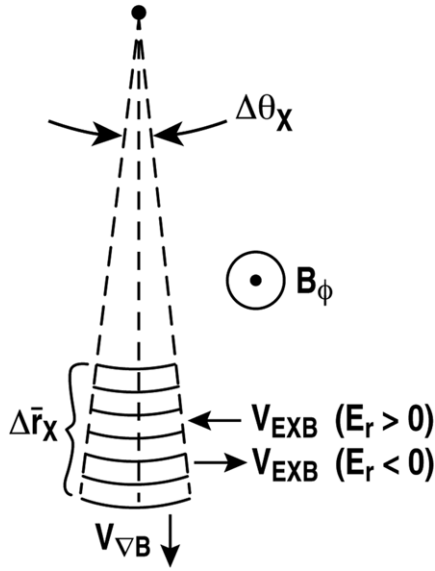
**Figure 16.** Idealized X-region for DIII-D lower single-null divertor configuration with $B_\phi$ out of the page and the plasma current into the page. Ions with $V \cdot B_\phi > 0$ will spiral poloidally counter-clockwise about the plasma centre (dot); ions with $V \cdot B_\phi < 0$ will spiral clockwise.

not spiral about the tokamak to provide the usual neoclassical cancellation of drift effects. Whereas ions quite rapidly move poloidally over the remainder of the flux surface outside of this 'X-region' by following along spiraling field lines, as the ions approach the X-point their poloidal motion is provided only by the slower poloidal $E_r \times B_\phi$ drift due to the radial electric field. If this $E_r \times B_\phi$ drift is in the same direction as the poloidal motion of the spiral along the field lines, then the ion will drift into the X-region. For the standard DIII-D configuration of current in the counter-clockwise direction and toroidal field in the clockwise direction, looking down from above the tokamak, co-current ions will drift into the X-region (depicted in figure 16) when $E_r > 0$, and counter-current ions will drift into the X-region when $E_r < 0$. This poloidal $E_r \times B_\phi$ drift will then move the ions poloidally across the null-$B_\theta$ region near the X-point until they again enter a plasma region in which $B_\theta \approx \varepsilon B_\phi$, where they once again can move rapidly poloidally over the flux surface by following the spiraling field lines.

More generally, when the toroidal magnetic field and the toroidal current are anti-parallel, the counter-current ions will drift into the X-region when $E_r < 0$, and the co-current ions will drift into the X-region when $E_r > 0$. When the toroidal magnetic field and plasma current are parallel, the counter-current ions will drift into the X-region when $E_r > 0$, and the co-current ions will drift into the X-region when $E_r < 0$.

However, while the ions are slowly drifting poloidally across the null-$B_\theta$ X-region near the X-point, they are also drifting vertically due to curvature and grad-$B$ drifts. In the usual DIII-D configuration with the toroidal field in the clockwise direction (looking down from above) and the plasma current in the counter-clockwise direction, and with a lower single-null divertor, this vertical drift is downward towards the divertor. If the time required for the ion to grad-$B$ and curvature drift downward across the separatrix is less than the

time required for the ion to $E_r \times B_\phi$ drift across the $B_\theta \ll \varepsilon B_\phi$ X-region near the X-point, the ion will be lost across the separatrix. Even if the ion is not lost across the separatrix, it will be displaced radially outward while it is traversing the null-$B_\theta$ region.

The poloidal magnetic field vanishes at the X-point, $B_\theta = 0$, and slowly increases to $B_\theta \approx \varepsilon B_\phi$ over a poloidal arc distance $r_{sep}(\theta_x)(\Delta\theta_x/2)$ on either side of $\theta = \theta_x$; i.e. $(1/r_{sep}(\theta_x))(\partial B_\theta/\partial\theta) \times r_{sep}(\theta_x)(\Delta\theta_x/2) \approx \varepsilon B_\phi$. The poloidal field also increases away from the X-point in the radial direction to $B_\theta \approx \varepsilon B_\phi$ over a distance $\Delta r_x$, i.e. $(\partial B_\theta/\partial r) \times \Delta r_x \approx \varepsilon B_\phi$. The solenoidal law $0 = \nabla \cdot B_\theta \approx (\partial B_\theta/\partial r) + (1/r)(\partial B_\theta/\partial r)$ relates the radial and poloidal variations of $B_\theta$ in the vicinity of the X-point. Combining these results leads to $(\Delta r_x/r_{sep}(\theta_x)\frac{1}{2}\Delta\theta_x) \approx 1$.

We represent the X-region as a tall wedge, or trapezoidal-shaped, region with its based centred on the X-point and extending radially inward (upward) a distance $\Delta r_x$ with width $r(\theta_x)\Delta\theta_x$, as depicted in figure 16. Within this region the motion of ions is determined by the radially outward (downward) curvature and grad-$B$ drifts and by the poloidal $E_r \times B_\phi$ drift. While the ion is $E_r \times B_\phi$ drifting across the null-$B_\theta$ region it is also grad-$B$ and curvature drifting radially outward (downward). The time required for an ion entering the plasma at radius $r$ to grad-$B$ and curvature drift downward a distance $\Delta r$ is

$$\tau_{\nabla B} = \frac{\Delta r}{V_{\nabla B,c}} = \frac{\Delta r}{(W_\perp + 2W_\parallel)/eRB} = \frac{eRB}{W(1+\zeta^2)}\Delta r, \quad (23)$$

where $\zeta$ is the average cosine of ion direction with respect to the magnetic field and $W$ denotes the ion energy. During this time the ion is also $E_r \times B_\phi$ drifting through a poloidal arc distance

$$r(\theta_x)\Delta\theta = V_{E\times B}\tau_{\nabla B} = \frac{E_r(r)}{B_\phi}\frac{eRB}{W(1+\zeta^2)}\Delta r. \quad (24)$$

Note that when the radial electric field changes sign the directions of the poloidal $E_r \times B_\phi$ drift and of the angular displacement both reverse.

We calculate the X-transport for an ion that $E_r \times B_\phi$ drifts into the X-region at a given radial location $r < r_{sep}$ by dividing the radius from the centre of the plasma to the separatrix into increments $\Delta r_n$ over each of which the plasma properties are approximated as constant, which allows the calculation of the change

$$\Delta\theta_n \simeq \frac{\Delta r_n}{r_n}\frac{eRE_{rn}}{W(1+\zeta^2)} \quad (25)$$

in $\Delta\theta$ that will take place while the ion grad-$B$ drifts radially downward (outward) a distance $\Delta r_n$.

Thus, the determination of the radial transport of an ion that enters the X-region is just a matter of calculating $\Delta\theta_n$ successively for all regions between the radius of entry and the separatrix and summing. If the calculated sum becomes greater than $\Delta\theta_x$, then the ion has drifted out of the X-region back into the plasma at that radius. Note that if an ion poloidally $E_r \times B_\phi$ drifts into the X-region in one direction and then grad-$B$ drifts into a region in which the electric field changes sign, then the $E_r \times B_\phi$ drift direction also changes poloidal direction. A change in sign of the summed $\Delta\theta_n$ indicates that

the ion has drifted out of the X-loss region on the same side on which it entered. Because $\Delta\theta_n$ is inversely proportional to the ion energy, the amount of X-transport is greater for higher energy ions.

The times required for ions to spiral poloidally around the flux surface by following along the field lines and to then $E_r \times B_\phi$ drift into the X-regions are short compared with the time required for the ions to flow radially outward (at about $1 \, \mathrm{m\,s^{-1}}$) across the flux surfaces. This implies that as the plasma flows radially outward across the flux surfaces the ion population is repeatedly swept through the X-region as the radial location increases, so that those ions entering the X-region at radius $r$ with energies equal to the energy needed for X-drift transport to radius $r'$ are immediately transferred to radius $r'$, where they drift poloidally out of the X-region back into the plasma at that radius $r'$.

This X-transport can be incorporated into the fluid calculations of ion particle and energy fluxes from equations (1) and (11) in two different ways. Particle and energy loss terms can be constructed to represent the particles and energy that have been X-transported from radius $r$ to all larger radii $r'$. Similarly, particle and energy sources can be calculated to represent the particles and energy that have been X-transported to radius $r'$ from all lesser radii $r$. These sources and sinks can be included directly in the particle and energy flux calculations. Alternatively, radially cumulative particle ($F_x$) and energy ($E_x$) loss fractions to account for those ions which have drifted across the separatrix can be defined similarly to the ion-orbit loss fractions discuss previously [27].

Summarizing, an ion in the plasma at any location other than the 'X-region' is assumed to spiral poloidally towards the 'X-region' (that small region extending radially inward from the X-point in which $B_\theta \ll \varepsilon B_\phi$). When this ion arrives at the boundary of the X-region it will $E_r \times B_\phi$ drift either into the X-region or back into the plasma, depending on the direction of $E_r$. If the ion drifts into the X-region, it will $E_r \times B_\phi$ drift across it, while grad-$B$ and curvature drifting downward (radially outward). If the ion reaches the other side of the X-region or, because of $E_r$ sign reversal, returns to the side on which it entered before it can drift across the separatrix, it returns to the plasma region at a larger radius—is 'X-transported'. If, on the other hand, the ion drifts across the separatrix at the X-point before it $E_r \times B_\phi$ drifts across the X-region to re-enter the plasma, it is 'X-lost' through the X-point into the divertor. The ions in the X-region are considered to be collisionless, in the present model. Once the ions return to the plasma, they are assumed to have collisions and equilibrate to a Maxwellian with the local (radial) ion temperature; then return to the X-region, etc. The ions in the plasma outside the X-region are considered to participate in neoclassical and other transport, and to undergo ion-orbit loss.

### 5.3. Effect of ion-orbit loss and X-transport on the interpretation of experimental heat diffusivities

As an illustrative example of the importance of ion-orbit loss and X-loss, their effect on the ion thermal diffusivity interpreted from experimental data using equation (14) has been evaluated for the DIII-D RMP shot #123301 discussed previously. The total ion radial particle flux was evaluated
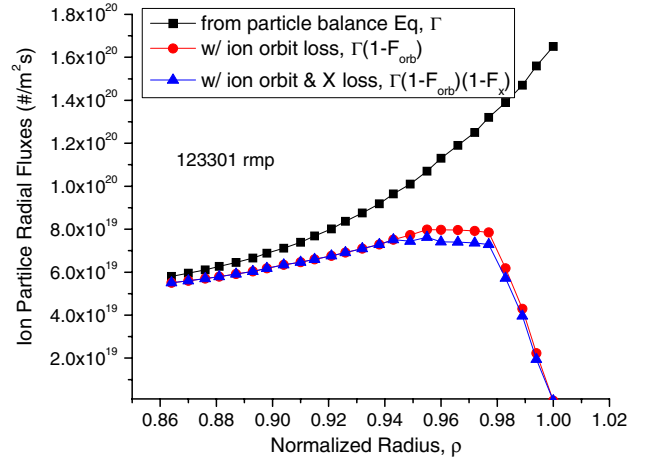


**Figure 17.** Convective and diffusive ion particle fluxes calculated from the ion particle balance equation, with and without correction for ion-orbit loss and X-loss.
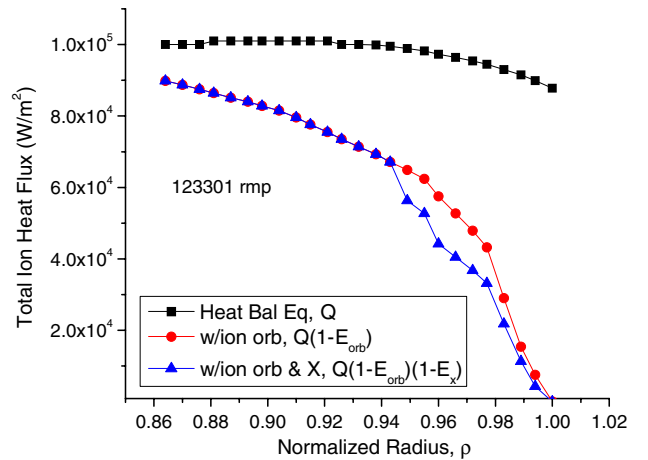


**Figure 18.** Total ion conductive and convective heat fluxes calculated from the ion heat balance equation, with and without correction for ion-orbit and X-loss.

by solving equation (1), using experimental data, for $\Gamma_j$; the total ion heat flux was evaluated by solving equation (11) for $Q_j$ (and equation (12) for $Q_e$); then using the ion-orbit loss fractions $F_{orb}$ and $E_{orb}$ shown in figure 14 to reduce the ion particle and energy fluxes; and finally using similarly calculated X-drift loss fractions $F_x$ and $Q_x$ discussed in the previous section to further reduce the ion particle and energy fluxes to the level that must be accounted for by other transport processes taking place in the plasma.

The total radial particle flux, $\Gamma_j$; the total radial particle flux reduced by the fraction carried by free-streaming ions lost across the separatrix, $\Gamma_j(1 - F_{orb})$; and the latter quantity also reduced by ions that X-drifted across the separatrix, $\Gamma_j(1 - F_{orb})(1 - F_x)$; are all shown in figure 17. Similar quantities related to the total ion energy are shown in figure 18.

Finally, the experimental ion thermal diffusivity that would be inferred from equation (14) using these different total particle and energy fluxes and the measured ion temperature and electron density profiles were calculated. Figure 19 shows the values of the ion thermal diffusivity that would be inferred (i) if ion-orbit loss and X-drift loss were ignored and only
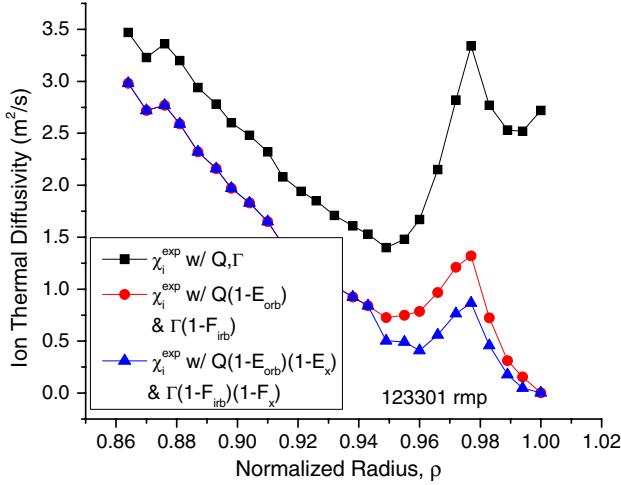
**Figure 19.** Ion thermal diffusivities interpreted from the measured ion temperature profile given in figure 3 using equation (24) and the heat fluxes of figure 5 with and without ion-orbit loss.



**Figure 20.** Inferred experimental ion thermal diffusivities with and without making ion-orbit loss corrections to the ion particle and heat fluxes.



**Figure 21.** Ion particle fluxes with and without reduction to account for X-transport and ion-orbit loss.

ion conductive and convective transport were assumed to be involved (solid square symbols); (ii) if the total ion fluxes were reduced to take into account ion-orbit loss to determine the conductive and convective ion fluxes to be used in equation (14) (solid circle symbols); and (iii) if the ion fluxes were further reduced to also take into account X-loss (solid triangle symbols). Taking into account the ions that are loss due to ion-orbit effects dramatically reduces the inferred ion thermal diffusivity in the steep-gradient region. (We note that these estimates are upper limits because some of the ions that cross the separatrix will return into the plasma.) Further taking into account ions that are lost due to X-drift causes a small further reduction in the ion thermal diffusivity in this DIII-D shot. Clearly, ion-orbit loss is a significant particle and energy transport mechanism in the DIII-D edge plasma.

Orbit loss fractions also have been calculated for the L-mode and H-mode phases of shot 118897 and used to correct the total ion heat and particle fluxes used to interpret the ion thermal diffusivities from the measured densities and temperatures using equation (14). The inferred experimental thermal diffusivities are shown in figure 20. The ion-orbit loss corrections are clearly important in the edge for the L-mode phase, completely changing the conclusion to be drawn about how the thermal diffusivity changes as the separatrix is approached, but have only a small effect on the H-mode interpretation. The relatively flat ion thermal diffusivity inferred in this early (ELM-free) H-mode phase is interesting in showing no evidence of an edge 'transport barrier'.

### 5.4. Effect of X-transport on the composition of the radial ion flux

For the H-mode discharge 123302, the minimum energy required for X-transport (i.e. the minimum energy required to make $\Delta\theta_n$ (or the sum of several successive $\Delta\theta_n$'s) less than the angular width $\Delta\theta_x$ of the X-region was proportional to the magnitude of the radial electric field at that radial location (see equation (25)). The radial electric field (shown in figure 10) was negative over almost the entire X-region, except just inside the separatrix, so the ions had to $E_r \times B_\phi$ drift across the entire
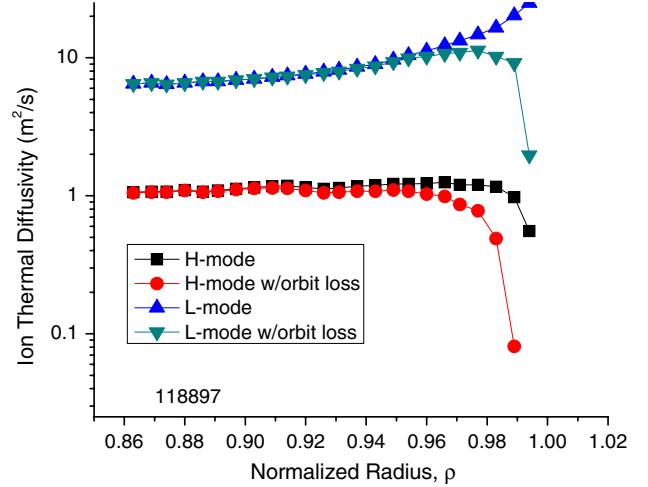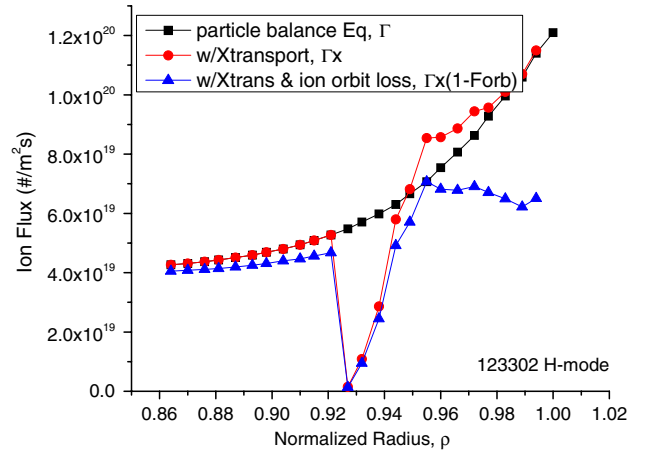
angular width $\Delta\theta_x$ of the X-region in order to re-enter the plasma.

The ion particle and heat fluxes for the H-mode discharge 123302 were evaluated using experimental data. Three cases were considered: (i) the X-transport ignored; (ii) X-transport source and sink terms [28] were evaluated and included in the particle and energy balance equations; and (iii) the X-transport terms source and sink terms were included in the balance equations and 'standard' ion-orbit loss fractions [27] $F_{orb}$ and $E_{orb}$ were used to further reduce the fluxes calculated by fluid theory. These results are shown for the ion particle flux in figure 21. (Note that the 'X-transport' from inward to outer flux surfaces is used in the calculation of the particle flux, as discussed following equation (25), in this figure, whereas in figures 17–19 the 'X-loss' fraction calculated in a manner similar to equations (20)–(22) was used.) The curve indicated by the square symbols shows the total outward particle flux; the curve indicated by the circles shows this total particle flux reduced by the particles that are being X-transported and therefore are not available to participate in other transport processes in the plasma; and the curve indicated by triangle symbols indicates the particle flux available to participate in

transport processes in the plasma after taking into account both X-transport and ion-orbit loss. With reference to figure 10, there is a large increase in X-transport where the radial electric field becomes negative between $\rho = 0.92$ and 0.93, and there is a large increase in ion-orbit loss beyond $\rho = 0.95$, both of which reduce the fraction of the particle flux that is being transported radially outward by conductive and other convective transport processes in the plasma.

*5.5. Intrinsic toroidal rotation in edge pedestal due to ion-orbit loss and X-loss*

The momentum loss fraction $M_{orb}$ (intermediate between $F_{orb}$ and $E_{orb}$ in figure 14) represents a loss of particles with toroidal velocity in the direction of the toroidal magnetic field (counter-current in these shots, with $B_{\phi}$ in the clockwise direction looking down and $I_{\phi}$ in the counter-clockwise direction), which would result in a net toroidal velocity in the edge pedestal in the direction ($\zeta_0 < 0$) of the particles which are not lost; i.e. in a counter-$B_{\phi}$ or co-current direction for these shots.

It can be shown that it is the counter-current ions which banana orbit outside the flux surface and are preferentially lost, independent of the direction of either the current or the toroidal magnetic field, producing an intrinsic rotation in the co-current direction. This result is consistent with the general finding of a co-current intrinsic $V_{\phi}$ in the edge pedestal of H-mode discharges in DIII-D [20] and other tokamaks, which supports the suggestion of [20] that ion-orbit loss could be the cause of the observed intrinsic toroidal rotation in the co-current direction in H-mode discharges.

The X-loss mechanism can also induce intrinsic co-current rotation in the edge pedestal in the standard DIII-D configuration considered in this paper. In the standard DIII-D configuration (current counter-clockwise and toroidal magnetic field clockwise, looking down on the tokamak—see figure 16) counter-current ions will spiral counter-clockwise poloidally to approach the X-region on the inboard side; they will drift into the X-region (and perhaps be lost) if $E_r < 0$, thereby leaving a surplus of co-current ions that would constitute intrinsic co-current rotation. Co-current ions, on the other hand, will spiral clockwise poloidally to approach the X-region on the outboard side; they will drift into the X-region if $E_r > 0$. For the H-mode discharges 123302 and 118897, $E_r < 0$ over the edge pedestal region, implying that the intrinsic rotation produced by X-loss would be in the co-current direction. On the other hand, for the L-mode phase of shot 118897 $E_r > 0$, indicating that it is the co-current ions that would be X-lost, leaving a surplus of counter-current ions to produce an intrinsic counter-current rotation. These results are generally consistent with experimental observations.

More generally, when the toroidal magnetic field and toroidal current are anti-parallel, the counter-current ions will drift into the X-region when $E_r < 0$, and the co-current ions will drift into the X-region when $E_r > 0$, resulting in intrinsic counter current rotation. On the other hand, when the toroidal magnetic field and current are parallel, the counter-current ions will drift into the X-region when $E_r > 0$, and the co-current ions will drift into the X-region when $E_r < 0$.

We plan to follow up on these observations in future work.

## 6. Summary and conclusions

There are (at least) two classical mechanisms for non-diffusive transport in the edge plasma: (i) a particle 'pinch' due to $V \times B$, $E_r$, etc forces and (ii) outward drifts (ion-orbit loss, X-transport). New methods were assembled for the treatment of these non-diffusive transport mechanisms within fluid theory. This new theoretical formulation was applied to interpret DIII-D experiments to provide insight as to the importance of the various non-diffusive transport mechanisms in DIII-D. Several important conclusions are summarized below.

Momentum balance requires that the radial particle flux is 'pinch-diffusive'; i.e. has a non-diffusive component produced by the radial electric field, $V \times B$ and lesser forces, as well as a 'diffusive' component produced by the pressure gradient force. This theoretical conclusion is supported by the experimental observation of an inward ion particle flux during the edge density buildup after an ELM crash.

Momentum balance requirements also define the particle diffusion coefficient in the plasma edge in terms of the interspecies collisional momentum transfer frequency and the toroidal angular momentum transport frequencies due to viscosity, charge-exchange, any anomalous effects, etc. Composite angular momentum transport frequencies can be interpreted from experiment.

The inward particle pinch associated with $V \times B$ and $E_r$ forces is more important than the ionization of recycling neutrals in determining the pressure profile in the edge plasma of several DIII-D H-mode discharges.

The particle 'pinch' is small and outward in the L-mode phase, but becomes large and inward in the H-mode phase of one DIII-D discharge, due primarily to the creation of the large negative well in $E_{rad}$ in H-mode. The diffusion coefficients in the L- and H-mode phases were similar in the steep-gradient region, implying that the steeper density gradient observed in H-mode is required (by momentum balance) in order to balance the larger inward pinch velocity, relative to L-mode, needed to provide the net outward radial particle flux required to satisfy the continuity equation. Thus, the improved particle confinement in H-mode relative to L-mode seems to be associated with a reversal of the outward L-mode pinch velocity to a strong inward H-mode pinch velocity, rather than to a reduction in particle diffusion coefficient. In fact, previous interpretations of a reduction in diffusion coefficients, leading to the postulation of a 'particle transport barrier', would seem to be an artefact of neglecting this pinch velocity.

RMP reduces the $E_r$ well relative to H-mode, thereby reducing the inward particle pinch in the edge plasma with RMP relative to an otherwise similar H-mode. Diffusion coefficients were similar for these RMP and H-mode discharges, so the reduction in inward pinch is apparently a significant contributor to the 'density pump-out' observed with RMP. Another significant contribution is the larger ion-orbit loss in the RMP than in the otherwise similar H-mode discharges because of the different electrostatic potential profiles.

Ion-orbit loss substantially reduces the parts of the total ion particle and energy fluxes that should be include in the interpretation of thermal diffusivities in the steep-gradient

region of the edge pedestal, thereby significantly reducing the ion thermal diffusivity interpreted from measurements of ion temperature profiles by using these total energy and particle fluxes.

The outward curvature and grad-$B$ drift of ions on field lines that are trapped poloidally in the vicinity of the X-point may be an important mechanism both for non-diffusive transport and for determining the radial electric field in the edge plasma. Further quantitative evaluation of this X-loss mechanism will be performed in the future.

Preferential ion-orbit loss and X-loss of counter- or co-current flowing ions produces an intrinsic co- or counter-current net toroidal rotation in the edge pedestal of DIII-D discharges, with the direction depending on whether the plasma current and toroidal magnetic field are parallel or anti-parallel. Further quantitative evaluation of this intrinsic rotation mechanism will be performed in the future.

## Appendix A. Torque representation

In order to evaluate the flux surface average (FSA) toroidal component of the momentum equation it is necessary to evaluate the FSA toroidal viscous torque and inertial terms in that equation. The neoclassical viscous torque can be written as the sum of 'parallel', 'gyroviscous', and 'perpendicular' components. Since the FSA of the 'parallel' component of the toroidal viscous torque vanishes identically, the flux surface averaged toroidal viscous torque may be written as the sum of the 'gyroviscous' and 'perpendicular' components

$$\langle R^2 \nabla \phi \cdot \nabla \cdot \Pi \rangle = \langle R^2 \nabla \phi \cdot \nabla \cdot \Pi \rangle_{\mathrm{gv}} + \langle R^2 \nabla \phi \cdot \nabla \cdot \Pi \rangle_{\perp}, \quad (A1)$$

where

$$\langle R^2 \nabla \phi \cdot \nabla \cdot \Pi \rangle_{\mathrm{gv}} = -\left\langle \frac{1}{R h_p} \frac{\partial}{\partial l_\psi} \left( R^3 h_p \eta_4 \frac{\partial}{\partial l_p} (V_\phi/R) \right) \right\rangle \quad (A2)$$

and

$$\langle R^2 \nabla \phi \cdot \nabla \cdot \Pi \rangle_{\perp} = -\left\langle \frac{1}{R h_p} \frac{\partial}{\partial l_\psi} \left( R^3 h_p \eta_2 \frac{\partial}{\partial l_\psi} (V_\phi/R) \right) \right\rangle \quad (A3)$$

in a right-hand $(\psi, p, \phi)$ toroidal flux surface coordinate system, where $\eta_2 = nT\tau/(\Omega\tau)^2$ and $\eta_4 \approx (\Omega\tau)\eta_2 \approx (10^3\text{–}10^4)\eta_2$, where $\Omega \equiv ZeB/m$ and $\tau$ is the collision frequency, so that the 'gyroviscous' toroidal torque is generally a couple of orders of magnitude larger than the 'perpendicular' toroidal viscous torque. Approximating the flux surface geometry by toroidal geometry and making a low order Fourier expansion $X(r, \theta) = X^0(r)[1 + X^c \cos\theta + X^s \sin\theta]$ for the densities and rotation velocities allows equations (A2) and (A3) to be written in a form exhibiting an explicit momentum transfer frequency

$$\langle R^2 \nabla \phi \cdot \nabla \cdot \Pi \rangle_{\mathrm{gv}\,j} \approx \frac{1}{2} \eta_{4j} \frac{r}{R_0} (L_n^{-1} + L_T^{-1} + L_{\upsilon_\phi}^{-1})$$
$$\times [(4 + \tilde{n}_j^c) \tilde{V}_{\phi j}^s + \tilde{n}_j^s (1 - \tilde{V}_{\phi j}^c)] V_{\phi j} \equiv R_0 n_j^0 m_j \nu_{\mathrm{gv}\,j} V_{\phi j} \quad (A4)$$

and

$$\langle R^2 \nabla \phi \cdot \nabla \cdot \Pi \rangle_{\perp j} \approx R_0 \eta_{2j} \left[ L_{\upsilon_\phi}^{-1} \left( \frac{1}{r} - L_{\eta_2}^{-1} \right) - \frac{1}{V_{\phi j}} \frac{\partial^2 V_{\phi j}}{\partial^2 r} \right]$$
$$\times V_{\phi j} \equiv R_0 n_j^0 m_j \nu_{\perp j} V_{\phi j} \quad (A5)$$

where the poloidal asymmetry coefficients $\tilde{n}_j^c \equiv n_j^c/\varepsilon$, etc can be determined by solving the low order Fourier moments of the poloidal component of the momentum balance.

Turbulent, or 'anomalous', toroidal viscous torque is usually assumed to be of the form of equation (A3) with an enhanced viscosity coefficient $\eta_{\mathrm{anom}}$, leading to

$$\langle R^2 \nabla \phi \cdot \nabla \cdot \Pi \rangle_{\mathrm{anom}\,j} \approx R_0 \eta_{\mathrm{anom}\,j} \left[ L_{\upsilon_\phi}^{-1} \left( \frac{1}{r} - L_{\eta_2}^{-1} \right) \right.$$
$$\left. - \frac{1}{V_{\phi j}} \frac{\partial^2 V_{\phi j}}{\partial^2 r} \right] V_{\phi j} \equiv R_0 n_j^0 m_j \nu_{\mathrm{anom}\,j} V_{\phi j}. \quad (A6)$$

Equation (1) can be used to write the inertial term in the FSA toroidal component of the momentum balance as

$$\langle R^2 \nabla \phi \cdot \nabla \cdot (n_j m_j \boldsymbol{V}_j \boldsymbol{V}_j) \rangle = \langle R^2 \nabla \phi \cdot n_j m_j (\boldsymbol{V}_j \cdot \nabla) \boldsymbol{V}_j \rangle$$
$$+ R_0 n_j m_j \nu_{\mathrm{ion}\,j} V_{\phi j} \quad (A7)$$

and the same set of approximations can be used to write the first term on the right as

$$\langle R^2 \nabla \phi \cdot n_j m_j (\boldsymbol{V}_j \cdot \nabla) \boldsymbol{V}_j \rangle \simeq \frac{1}{2} \left( \frac{V_{rj}}{R_o} \{\varepsilon(1 + \tilde{n}_j^c + \tilde{V}_{\phi j}^c) \right.$$
$$- 2 R_o L_{\upsilon_\phi j}^{-1}\} - \varepsilon \frac{V_{\theta j}^0}{R_o} \{\tilde{V}_{\phi j}^s (1 + \tilde{n}_j^c + \tilde{V}_{\theta j}^c) - \tilde{V}_{\theta j}^s (1 + \tilde{V}_{\phi j}^c)$$
$$\left. - \tilde{V}_{\phi j}^c \tilde{n}_j^s\} \right) n_j m_j R_0 V_{\phi j}^0 \equiv R_0 n_j m_j \nu_{nj} V_{\phi j}^0. \quad (A8)$$

## Appendix B. Generalized diffusion theory

The results of appendix A may be used to write the FSA toroidal component of the momentum balance (second moment) equation as

$$n_j^0 m_j \nu_{jk}^0 ((1 + \beta_j) V_{\phi j}^0 - V_{\phi k}^0) = n_j^0 e_j E_\phi^A + e_j B_\theta^0 \Gamma_{rj} + M_{\phi j}^0, \quad (B1)$$

where

$$\beta_j \equiv \frac{\nu_{\mathrm{gv}\,j}^0 + \nu_{\perp j}^0 + \nu_{\mathrm{anom}\,j}^0 + \nu_{nj}^0 + \nu_{elcxj}^0 + \nu_{\mathrm{ion}\,j}}{\nu_{jk}^0} \equiv \frac{\nu_{dj}^*}{\nu_{jk}^0}. \quad (B2)$$

Now, combining the radial and toroidal components of the FSA momentum balance equations— equations (3) and (B1)—yields a generalized pinch-diffusion relation for the radial particle flux of species '$j$':

$$\Gamma_{rj} \equiv \langle n_j V_{rj} \rangle = n_j D_{jj} (L_{nj}^{-1} + L_{Tj}^{-1})$$
$$- n_j D_{jk} (L_{nk}^{-1} + L_{Tk}^{-1}) + n_j V_{pj}, \quad (B3)$$

where the 'diffusion coefficients' are given by

$$D_{jj} \equiv \frac{m_j T_j (\nu_{dj}^* + \nu_{jk})}{(e_j B_\theta)^2}, \qquad D_{jk} \equiv \frac{m_j T_k \nu_{jk}}{e_j e_k (B_\theta)^2} \quad (B4)$$

and the 'pinch velocity' is given by

$$n_j V_{pj} \equiv -\frac{M_{\phi j}}{e_j B_\theta} - \frac{n_j E_\phi^A}{B_\theta} + \frac{n_j m_j \nu_{dj}^*}{e_j B_\theta} \left( \frac{E_r}{B_\theta} \right) + \frac{n_j m_j f_p^{-1}}{e_j B_\theta}$$
$$\times ((\nu_{jk} + \nu_{dj}^*) V_{\theta j} - \nu_{jk} V_{\theta k}). \quad (B5)$$

A sum over the '$k$' terms is understood when more than two ion species are present. The quantity $f_p^{-1} \equiv B_\phi/B_\theta$.

Subject to the assumption that there is a single impurity species '$k$' distributed with the same radial distribution and the same local temperature as the main ions (j), equation (B3) can be written as a constraint on the main ion pressure gradient given by equation (4).

## Appendix C. Multispecies generalized radial diffusion theory

Since diffusion theory is generally used to describe ion particle transport in plasma edge codes (e.g. [36, 37]), it is of interest to compare the radial transport theory implied by the above relations with the form of diffusion theory commonly used in the plasma edge codes. Using the generalized pinch-diffusion relation of equation (B3) in the continuity equation (1), which governs $\Gamma_{rj}$, yields the coupled set of generalized diffusion equations that determine the particle distribution in the edge plasma for ion species '$j$', $\nabla \cdot \boldsymbol{\Gamma}_j = S_j$, the radial component of which can be written for each species in the slab limit appropriate in the plasma edge

$$-\frac{\partial}{\partial r}\left(D_{jj}\frac{\partial n_j}{\partial r}\right) - \frac{\partial}{\partial r}\left(D_{jk}\frac{\partial n_k}{\partial r}\right) - \frac{\partial}{\partial r}\left(D_{jj}\frac{n_j}{T_j}\frac{\partial T_j}{\partial r}\right)$$
$$-\frac{\partial}{\partial r}\left(D_{jk}\frac{n_j}{T_k}\frac{\partial T_k}{\partial r}\right) + \frac{\partial(n_j V_{pj})}{\partial r} = S_j. \quad (C1)$$

Again, the '$jk$' subscript indicates a sum over '$k$'. Note that the 'self-diffusion' coefficient $D_{jj}$ involves all the momentum transport rates for species '$j$' (i.e. atomic physics, viscous, anomalous, etc as well as the interspecies collisional momentum exchange frequency for species '$j$'). There is an equation (C1) for each ion species in the plasma, and they are coupled.

The generalized diffusion theory of equation (C1), which was rigorously derived from momentum balance and the continuity equation for each ion species in the plasma, is different in several respects from the usual ad hoc form of diffusion theory (equation (C1) but retaining only the first term on the left side) that is commonly used to represent radial particle transport in plasma edge fluid codes. First, the diffusion equation for species '$j$' depends not only on the density gradient of species '$j$', but on the density gradients for all other ion species as well. Second, the diffusion equation for species '$j$' depends on the temperature gradients for all ion species. This implies that, when used in the predictive mode, the diffusion equations for all the ion densities and the heat balance equations for all the ion temperatures are coupled and must be solved simultaneously.

The third major difference is that there is a convection term with a pinch velocity (equation (B5)) that depends on the poloidal rotation velocities for all the ion species and on the radial electric field, the induced toroidal electric field, and the neutral beam (or any other) external momentum input or torque. As discussed above, we have found that the pinch velocity was the dominant term in the pinch-diffusion relation insofar as the determination of the edge density profile. Thus, we anticipate that the convective last term on the left in equation (C1) will have a major effect on the calculation of the ion particle profile in the edge plasma. This implies that when equation (C1) is used in the predictive mode, the rotation equations must also be solved simultaneously with the particle and heat diffusion equations.

## Acknowledgments

The authors would like to acknowledge the contributions of the DIII-D team in the measurement and reduction of the

## References

[1] Hubbard A.E. 2000 *Plasma Phys. Control. Fusion* **42** A15
[2] Maggi C.F. 2010 *Nucl. Fusion* **50** 066001
[3] Kotschenreuther M. *et al* 1997 *Proc. 16th Conf. Plasma Physics Controlled Fusion Research (Montreal, Canada, 1996)* vol 2 (Vienna: IAEA) p 371
[4] Kinsey J.E., Waltz R.E. and Schissel D.P. 1997 *Proc. 24th European Physical Society Conf. (Berchtesgarten, Germany)* vol III (Geneva: EPS) p 1081
[5] Groebner R.J., Burrell K.H. and Seraydarian R.P. 1990 *Phys. Rev. Lett.* **64** 3015
[6] Stacey W.M. and Groebner R.J. 2010 *Phys. Plasmas* **17** 112512
[7] Stacey W.M. and Groebner R.J. 2011 *Nucl. Fusion* **51** 063024
[8] Stacey W.M. and Evans T.E. 2011 *Nucl. Fusion* **51** 013007
[9] Snyder P.B., Wilson H.R., Ferron J.R., Lao L.L., Leonard A.W., Osborne T.H., Turnbull A.D. and Xu X.Q. 2004 *Nucl. Fusion* **44** 320
[10] Biglari H., Diamond P.H. and Terry P.W. 1989 *Phys. Fluids* B **2** 1
[11] Burrell K.H. 1997 *Phys. Plasmas* **4** 1499
[12] Terry P.W. 2000 *Rev. Mod. Phys.* **72** 109
[13] Hinton F.L. and Chu M. 1985 *Nucl. Fusion* **25** 345
[14] Miyamoto K. 1996 *Nucl. Fusion* **36** 927
[15] Shaing K.C. and Crume E.C. 1989 *Phys. Rev. Lett.* **63** 2369
[16] Shaing K.C., Crume E.C. and Houlberg W.A. 1990 *Phys. Fluids* B **2** 1492
[17] Shaing K.C. 1992 *Phys. Fluid* B **4** 171
[18] Shaing K.C. 2002 *Phys. Plasmas* **9** 1
[19] Matthews G.F., *et al* 2002 *JET Report* EFDA-JET-CP(02)01-02
[20] DeGrassie J.S., Groebner R.J., Burrell K.H. and Solomon W.M. 2009 *Nucl. Fusion* **49** 085020
[21] Chang C.S., Kue S. and Weitzner H. 2002 *Phys. Plasmas* **9** 3884
[22] Chang C.S., Kue S. and Weitzner H. 2004 *Phys. Plasma* **11** 2649
[23] Weitzner H. and Chang C.S. 2004 *Phys. Plasmas* **11** 3060
[24] Chang C.S. 2004 *Phys. Plasmas* **11** 5626
[25] Hahn S.H., Ku S. and Chang C.S. 2005 *Phys. Plasmas* **12** 102501
[26] Chang C.S. and Ku S. 2008 *Phys. Plasmas* **15** 062510
[27] Stacey W.M. 2011 *Phys. Plasmas* **18** 102504
[28] Stacey W.M. 2011 X-transport of ions in diverted tokamaks, with application to DIII-D *Phys. Plasmas* **18** 122504
[29] Mahdavi M.A., Maingi R., Groebner R.J., Leonard A.W., Osborne T.H. and Porter G. 2003 *Phys. Plasmas* **10** 3984
[30] Groebner R.J., Mahdavi M.A., Leonard A.W., Osborne T.H., Wolf N.S., Porter G.D., Stangeby P.C., Brooks N.S., Colchin R.J. and Owen L.W. 2004 *Nucl. Fusion* **44** 204
[31] Snyder P.B., Groebner R.J., Leonard A.W., Osborne T.H. and Wilson H.R. 2009 *Phys. Plasmas* **16** 056118
[32] Callen J.D., Groebner R.J., Osborne T.H., Canik J.M., Owen L.W., Pankin A.Y., Rafiq T., Rognlien T.D. and Stacey W.M. 2010 *Nucl. Fusion* **50** 064004
[33] St. John H.E. *et al* 1995 *Proc. 15th Conf. Plasma Physics Controlled Fusion (Seville, Spain, 1994)* vol 3 (Vienna: IAEA) p 60

[34] Pereverzev G. and Yushmanov P.N. 2002 ASTRA automated system for transport analysis in a tokamak *Technical Report* IPP 5/98, Max-Planck Institut fur Plasmaphysik
[35] Stacey W.M. 1998 *Phys. Plasmas* **5** 1015
Stacey W.M. 2001 *Phys. Plasmas* **8** 3673
Stacey W.M. 2000 *Nucl. Fusion* **40** 965
[36] Rognlien T.D. and Rensink M.E. 2002 *Fusion Eng. Des.* **60** 497
[37] Schneider R., Bonnin X., Borrass K., Coster D.P., Kastelewicz H., Reiter D., Rozhansky V.A. and Braams B.J. 2006 *Contrib. Plasma Phys.* **46** 3
[38] Stacey W.M. 2008 *Phys. Plasmas* **15** 052503
[39] Luxon J. 2002 *Nucl. Fusion* **42** 614

[40] Stacey W.M. 2005 *Fusion Plasma Physics* (Weinheim: Wiley-VCH) pp 85–9
[41] Stacey W.M. 2008 *Contrib. Plasma Phys.* **48** 94
[42] Stacey W.M. and Groebner R.J. 2008 *Phys. Plasmas* **15** 012503
[43] Stacey W.M. and Groebner R.J. 2009 *Phys. Plasmas* **16** 102504
[44] Floyd J.-P. and Stacey W.M. 2012 Numerical investigation of extending diffusion theory codes to solve the generalized pinch-diffusion equations in the edge pedestal *Fusion Sci. Technol.* at press
[45] Chankin A. and McCracken G. 1993 *Nucl. Fusion* **33** 1459
[46] Azarenkov N. and Kononenko Zh. 2009 *J. Kharkiv Univ.* **859** 51